J. Fluid Mech. (1990), *vol.* 213, *pp.* 71–94
Printed in Great Britain

The von Neumann paradox for the diffraction of weak shock waves

By P. COLELLA AND L. F. HENDERSON†
Mail Stop L-316, Lawrence Livermore National Laboratory, P.O. Box 808, Livermore, CA 94550, USA

(Received 18 November 1988 and in revised form 23 June 1989)

We present results from our experiments with the irregular reflection of shock waves in argon. We compare the data with the results we obtained numerically; the assumptions for the computational code were that we had unsteady, two-dimensional, compressible, inviscid, flow of a perfect gas. When precautions were taken to reduce the effects of the gas viscosity on the experimental data, we obtained very good agreement between the numerical and the experimental results for the ramp Mach number and the trajectory path triple-point angle, but there were discrepancies with the wave-angle data. The discrepancies were ascribed to the sensitivity of the data to both viscosity and to a singularity. We show that there are actually two weak irregular wave reflections, namely a classic Mach reflection (MR) and a new type, that we call a von Neumann reflection (NR). The structure of the NR is discussed in some detail, and so are the transition criteria for the various wave systems.

1. Introduction

The regular reflection (RR), and the irregular, or Mach reflection (MR), of a plane shock wave i at a rigid surface was first discussed comprehensively by von Neumann (1943). He assumed that all the waves were shocks which obeyed the Rankine–Hugoniot (RH) jump conditions, and all were of negligible curvature and thickness. Although the theory was developed for a general equation of state, he gave most attention to air which he assumed to be a perfect gas.

He found that transition between RR and MR, denoted by, RR $\rightleftharpoons$ MR, could be brought about by a continuous change in a system parameter, such as, for example, the corner angle θ, or the inverse strength of i, $\xi_i \equiv P_0/P_1$, where P is the pressure and the subscripts 0, 1, refer to conditions upstream and downstream of i (figure 1). When he studied the conditions for transition, he found it necessary to distinguish between a strong and a weak incident shock i, because ξ_i determined the nature of the transition criterion. Using a property of the polar diagram, he was able to give a rigorous definition of the boundary between strong and weak shocks. In the special case of a perfect gas, the critical value of $\xi_i = \xi_{cr}$, depended only on the ratio of specific heats $\gamma \equiv C_p/C_v$, (table 1). However, an alternative definition which is physically more satisfactory has been given by Henderson & Siegenthaler (1980). In this case, i is strong if the flow downstream of its reflected shock r, is supersonic at, or near, transition, but it is weak when this flow is subsonic. Hence the strong/weak

† Permanent address: Department of Mechanical Engineering, University of Sydney, NSW 2006, Australia.

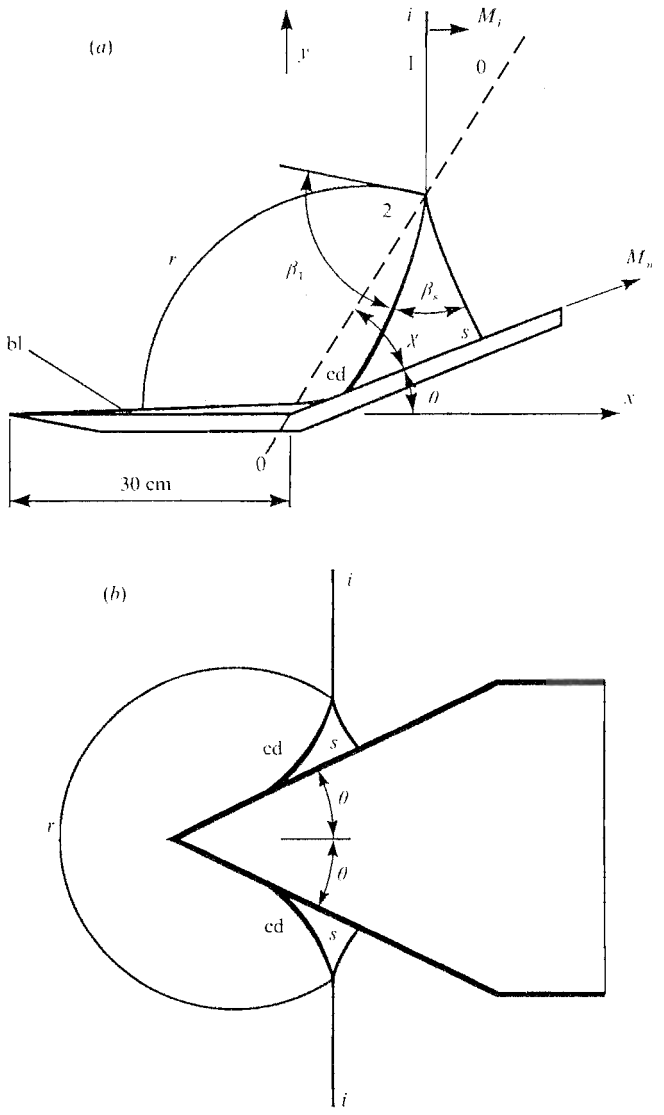

FIGURE 1. Mach reflection caused by the diffraction of a plane shock over a compression corner. (*a*) Concave corner model. (*b*) Symmetrical wedge model designed to reduce the effects of viscosity particularly at the corner. *i*, incident shock; *r*, reflected shock; *s*, Mach shock; cd, contact discontinuity; θ, corner angle; χ, trajectory path angle of wave triple point; M_n, shock Mach number of Mach shock along the ramp surface; β_1 angle of incidence of *i* with respect to the cd; β_s, wave angle of *s* with respect to the cd.

boundary is at the sonic flow point. The two definitions are close together for a perfect gas (see tables 1 and 2).

For weak shocks von Neumann concluded that transition took place at the detachment point. Subsequently, Hornung & Taylor (1982), proposed instead that transition occurred at the sonic point. Actually, these two criteria are too close together for present day experimental techniques to distinguish between them, so they will be referred to generically as the sonic/detachment point criterion. By contrast, when *i* was strong, von Neumann suggested that the mechanical

γ	$\frac{5}{3}$	$\frac{7}{5}$	$\frac{9}{7}$
$\xi_i = \xi_{cr}$	0.36385	0.43317	0.46504
M_i	1.5487	1.4565	1.4221
θ°	51.167	48.588	47.404

TABLE 1. Von Neumann separation conditions between strong and weak shocks

γ	$\frac{5}{3}$	$\frac{7}{5}$	$\frac{9}{7}$
$\xi_i = \xi_{cr}^*$	0.30375	0.37531	0.40855
M_i	1.6833	1.5577	1.5122
θ°	53.32	49.626	48.388

TABLE 2. Separation conditions between strong and weak shocks for $M_2 = 1$ (after Henderson & Siegenthaler)

equilibrium point was the correct criterion and it is now also called the von Neumann point.

When his theory was compared with experimental data obtained from shock waves in gases, the agreement was generally satisfactory provided that i was a strong shock. This conclusion applied to both stationary and self-similar (pseudostationary) flows, for both regular and Mach reflections, (Bleakney & Taub 1949; Kawamura & Saito 1956; Henderson & Lozzi 1975, 1979; Henderson & Gray 1982; Hornung & Robinson 1982). For strong shock reflection in steady state flow, experiments showed clearly that the von Neumann point was the correct transition criterion (Mölder 1971; Pantazapol, Bellet & Soustre 1972; Henderson & Lozzi 1975, 1979; Hornung & Kychakoff 1977, Hornung, Oertel & Sandeman 1979). The same conclusion applied to certain self-similar systems such as twin re-entry concave corners (Henderson & Lozzi 1975), but not necessarily to all self-similar systems, particularly to a plane shock i diffracting over a single concave (compression) corner. In this last case, which has been extensively studied, experiment indicates that regular reflection apparently persists not only beyond the von Neumann point but even beyond the sonic/detachment point, that is, into a region where, according to the von Neumann theory, RR is impossible.

When i was a weak shock, the cited references again showed that the theory agreed well with experiment for RR, except that once more RR apparently persisted beyond the sonic/detachment point. For weak Mach reflection the theory almost always failed to agree with experiment. In fact if i is sufficiently weak the von Neumann theory has no physically realistic solutions for MR, (Henderson 1987) even though experiments show that MR-like phenomena do in fact exist. This suggests of course that the physical model of weak MR used by von Neumann is then incorrect. The apparent persistence of either RR or MR into regions of parameter space $(\gamma \times \xi_i \times \theta)$, for which the theory has no physically realistic solutions is defined here to be the 'von Neumann paradox'. The term was first used by Birkhoff (1950, p. 24, 1st edition) although in a more restricted sense than by us.

The object of the present paper is to study the paradox with particular attention to the weak irregular reflection. First, we present the results of our experiments with weak shocks diffracting over concave (compression) corners (figure 1). In order to

keep the physics as simple as possible, we selected argon to be the compressible medium, which of course eliminated the effects of molecular vibration, rotation, and chemical reactions (Johannesen & Hodgson 1979). Secondly, we present the results of our computations of the flow fields of the experiments. For weak shocks, the flow downstream of an irregular wave system is by definition subsonic, so the von Neumann theory of it can only be applied to the immediate vicinity of the shock triple point. Our calculations, however, deal with the entire flow field. Like von Neumann, we assumed that the gas was perfect and inviscid and that the incident i, and Mach s, shock waves were of negligible thickness. In spite of this, our calculations are more general, not only because we compute the entire flow field, but also because we only require the reflection r to obey the RH jump conditions. In particular, this allows r to be either a shock of negligible thickness and curvature, as assumed by von Neumann, or, for example a subcritical compression of finite thickness which seems to occur in some parts of some flow fields.

Although the numerical data were found to agree with experiment within the limits of experimental error there were small systematic discrepancies. These were ascribed to shock–boundary-layer interaction effects arising from the viscosity of the argon. In order to test this idea some of the concave corner model experiments (figure 1*a*) were repeated with symmetric wedge models (figure 1*b*). These were designed to greatly reduce the shock–boundary-layer interaction at the concave corner. Some of the discrepancies then vanished completely, while others were substantially reduced.

Finally we shall present evidence that there are two types of weak irregular reflection. One is a classical Mach reflection (MR) and the other is a new type whose reflected disturbance is not a shock in the region of its interaction with the incident/Mach shocks, but is a curved band of unsteady, self-similar, compressions of finite thickness. The flow downstream of the reflection is non-uniform near the interaction region. We shall discuss the transition conditions between the various phenomena.

2. The experiments

These were done at the University of Sydney in a conventional shock tube which has been described elsewhere (Henderson & Gray 1981). The concave corner model used is illustrated in figure 1 (*a*). The working section of the tube was filled with argon for all the experiments, so the ratio of specific heats was a constant, $\gamma = \frac{5}{3}$. The inverse shock strength ξ_i was also held constant for a particular series of experiments. The only variable parameter was the corner angle θ, and it was changed in discrete steps between the sonic/detachment point $\theta = \theta^*$, and the glancing incidence point $\theta = 0°$, so $\theta^* \geqslant \theta \geqslant 0$. Evidently, the values of the parameter set (γ, ξ_i, θ) completely specified a particular flow field and its associated wave system at a given instant. By table 2, an irregular system was weak when $\xi_i > \xi_{cr} = 0.30375$, that is, when the shock Mach number M_i of i was $M_i < 1.683$. The incident wave speed was measured by piezoelectric transducers, and the wave systems were photographed with a conventional schlieren apparatus.

The angle β_1 between the reflected wave r, and the contact discontinuity cd, and β_s between cd and the Mach shock s were measured from the photographs. The contact discontinuity and all the waves except i are curved near the triple point so there was some uncertainty about where to draw the tangents at this point for the purpose of angle measurement. Accordingly the experimental error was a little larger for these weak shock systems than they are for strong systems where the waves are

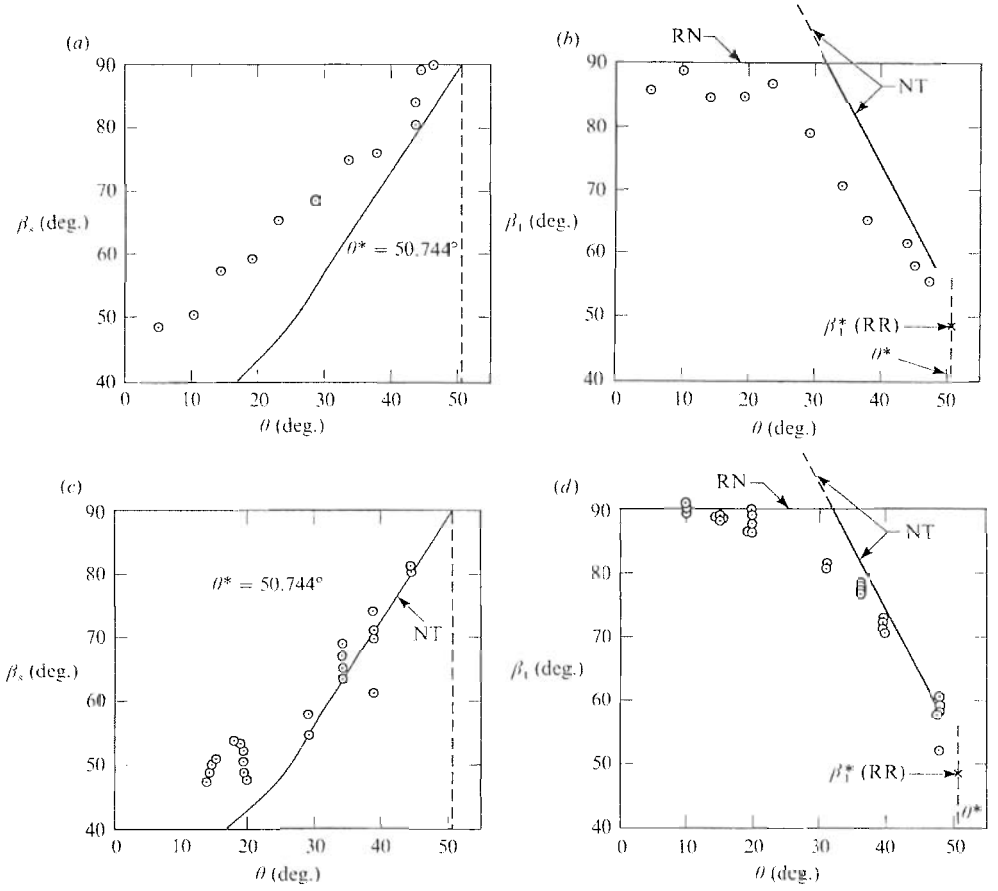

FIGURE 2. Comparison of the von Neumann theory of weak Mach reflection with experiments in argon. $\gamma = \frac{5}{3}$, $\langle \xi_i \rangle = 0.406$, $\langle M_i \rangle = 1.47$. (*a*, *b*) Experimental data for concave corner models, see figure 1 (*a*). (*c*, *d*) Experimental data for symmetrical (low viscosity effects) models, see figure 1 (*b*). NT, von Neumann theory of weak MR; RN, region of von Neumann reflection (NR) where $\beta_1 > \frac{1}{2}\pi$. ⊙, experimental data point. Experimental errors are negligible for θ_c and $\pm 2.0°$ approximately for (β_1, β_s).

either locally straight, or nearly so. We also measured the Mach number M_n, of the Mach shock along the sloping ramp where it is locally a normal shock, and the trajectory path angle χ of the triple point. The angle χ was measured as indicated in figure 1, that is on the assumption that the trajectory path of the triple point passed through the corner. The uncertainty in the measurements of (M_n, χ) is significantly less than for the wave angles (β_1, β_s) and we consider the former to be the most reliable and robust of all our data. The results for twelve experiments with an average $\langle \xi_i \rangle = 0.406$, or $\langle M_i \rangle = 1.47$, are presented in figures 2 (*a*, *b*) and 3 (*a*, *b*), and for four experiments with $\langle \xi_i \rangle = 0.919$, or $\langle M_i \rangle = 1.035$, are presented in figures 4 (*a*) and 4 (*b*).

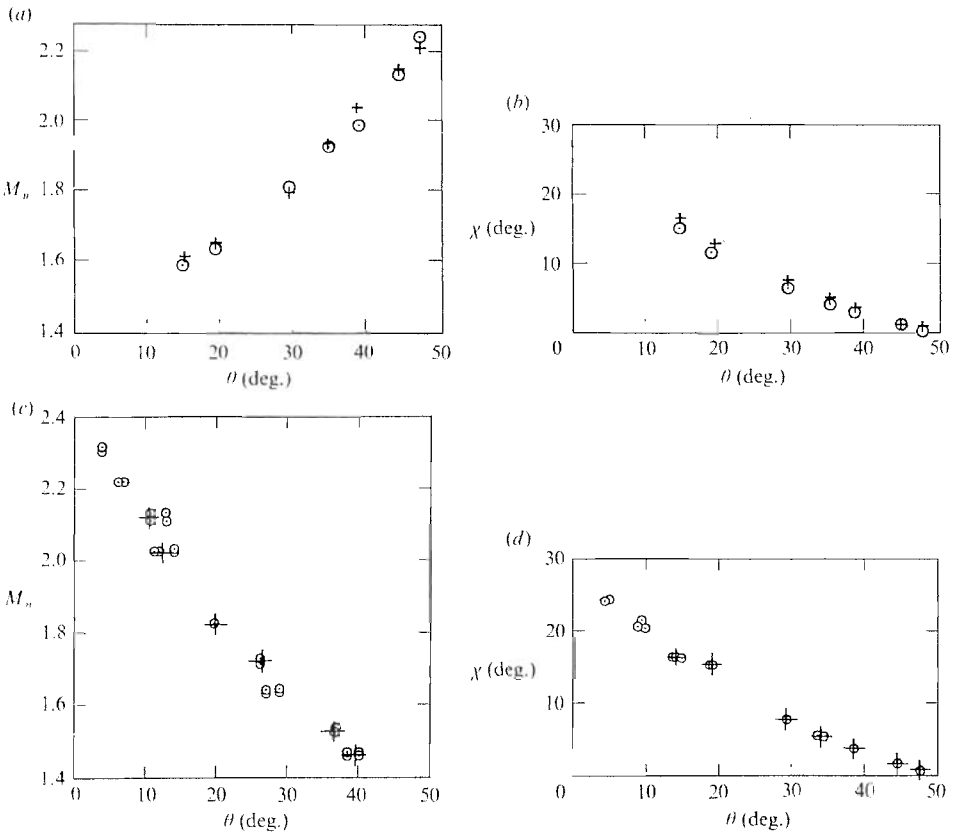

FIGURE 3. Comparison of the finite difference code calculations of weak irregular reflections with experiments in argon. $\gamma = \frac{5}{3}$. $\langle \xi_i \rangle = 0.406$. $\langle M_i \rangle = 1.47$. ($a$, b) Concave corner model experimental data. (c, d) Symmetrical (low viscosity effects) model data. +, numerical data from the code using the same (γ, ξ_i, θ) measured in the experiments. Experimental errors are negligible for θ. $M_n \pm 0.02$. $\chi \pm 1.25°$. Run numbers of the experiments in (a, b) are 81, 82, 84, 85, 86, 87, 100.

3. The computations

3.1. *The equations*

We considered the unsteady Euler equations and the continuity equation for the flow of a perfect, compressible, inviscid, gas in two dimensions, thus,

$$\left.\begin{aligned} \frac{\partial \rho}{\partial t} + \frac{\partial \rho u}{\partial x} + \frac{\partial \rho v}{\partial y} &= 0, \\ \frac{\partial \rho u}{\partial t} + \frac{\partial (\rho u^2 + P)}{\partial x} + \frac{\partial (\rho uv)}{\partial y} &= 0, \\ \frac{\partial \rho v}{\partial t} + \frac{\partial (\rho uv)}{\partial x} + \frac{\partial (\rho v^2 + P)}{\partial y} &= 0, \\ \frac{\partial \rho e}{\partial t} + \frac{\partial (\rho ue + uP)}{\partial x} + \frac{\partial (\rho ve + vP)}{\partial x} &= 0. \end{aligned}\right\} \tag{1}$$

where ρ is the density u, v, the x and y velocity components, and e is the total energy per unit mass. The pressure P may be obtained from the equation of state,

$$P = (\gamma - 1)\rho\,(e - \tfrac{1}{2}(u^2 + v^2)). \tag{2}$$

3.2. *The numerical method*

The code was developed at the Lawrence Livermore National Laboratory (LLNL) and run on a Cray 2 computer. It uses a finite difference method based on a rectangular grid in conjunction with a higher-order extension of Godunov's method of a type first introduced by van Leer (1979), and Colella & Woodward (1984). The method is accurate to second order in space and time, and captures shock waves and other discontinuities with minimal numerical overshoot and dissipation. Extensive use has been made of this method to compute unsteady shock reflections in gases involving complex interactions between discontinuities and smooth waves; it gives good agreement with experiment (Woodward & Colella 1984; Glaz *et al.* 1985).

The version of the method used by us is a single step unsplit method as described by Colella (1984). The numerical fluxes on the faces of the finite difference cells are all computed and differenced simultaneously rather than a pair at a time for each coordinate direction, as is done for the operator split version of the code (Colella & Woodward 1984).

Naturally we wanted to obtain as accurate and detailed a picture as possible of the shock interaction region, so we explored two other techniques which were aimed at increasing our resolution in the neighbourhood of the reflection point and the triple point. One of them was local refinement of the finite difference mesh, which is a simplified form of the ideas in Berger & Colella (1987). At any given time the density of the finite difference cells was increased by an integer factor, called the refinement ratio, in each coordinate direction. While the size of the rectangular region which was subject to refinement was fixed, the refined region was moved in such a way that the incident and Mach shocks in the neighbourhood of the reflecting wall, remained centred on the refined region. The second technique involved tracking the incident shock i, using the algorithm of Chern & Colella (1987). In this case i was represented by a polygonal curve which moved through the finite difference mesh with the Rankine–Hugoniot jump conditions, providing the flux boundary conditions for the finite difference calculations. The coupling behind the tracked front was fully conservative and employed finite volume differencing on either side of the front in cells intersected by the tracked front. This enabled us to compute discontinuities which were captured on the finite difference grid which intersected the tracked front. In particular, we treated the transition to Mach reflection as the formation and propagation of a kink along the incident shock with the reflected wave and the slip line computed as captured structures on the finite difference grid.

The use of both of these adaptive techniques improved the resolution of the finite difference calculation in several ways. Mesh refinement enabled us to focus the grid resolution on the small-scale structures in the neighbourhood of the reflection point. For example, when computing the transition between regular and Mach reflection, we were able to obtain Mach shocks whose height was only $\frac{1}{2}\%$ of the maximum vertical height of the reflected wave. It would have been prohibitively expensive to resolve such structures on a uniform grid. Front tracking eliminated some dynamic range problems associated with finite difference calculations of shocks, particularly in the presence of discontinuities in the mesh spacing.

3.3. *The computations*

These were organized as though we were doing a typical series of experiments with a compression corner in a shock tube (figure 1*a*); that is, both (γ, ξ_i) were held constant while the corner angle θ was varied in discrete steps. Then ξ_i was changed to a new value and the series was repeated.

Run no.	81	82	84	85	86	87	100
$\theta°$	14.58	19.30	29.27	34.60	38.68	44.48	47.55
ξ_i	0.403	0.414	0.406	0.409	0.405	0.400	0.400
M_i	1.48	1.46	1.47	1.47	1.47	1.48	1.48
Wave reflection	NR	NR	NR	MR	MR	MR	MR

TABLE 3. Measured values of the input parameters for shock waves reflecting off concave corners in argon, $\gamma = \frac{5}{3}$, $\langle \xi_i \rangle = 0.406$, $\langle M_i \rangle = 1.47$

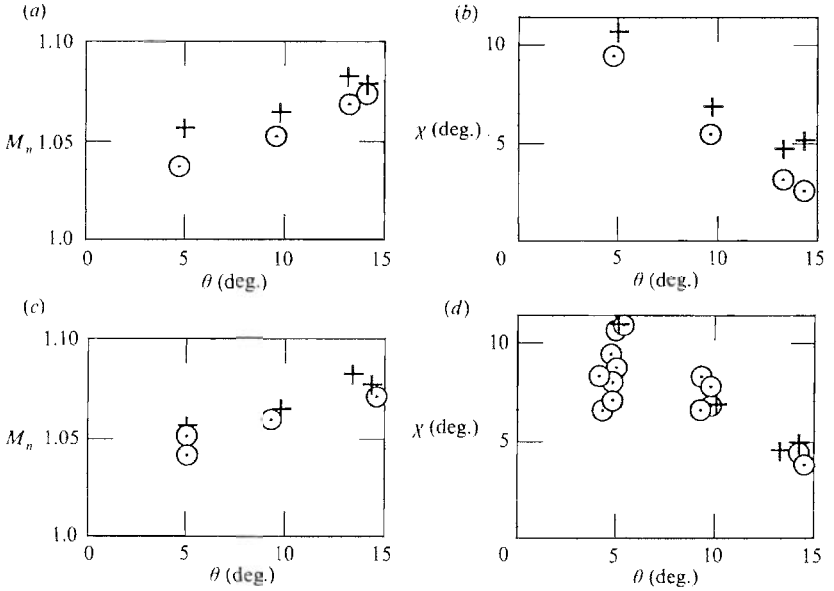

FIGURE 4. Comparison of the finite difference code calculations of weak irregular reflections with experiments in argon, $\gamma = \frac{5}{3}$, $\langle \xi_i \rangle = 0.919$, $\langle M_i \rangle = 1.035$. (*a*, *b*) Concave corner model experimental data. (*c*, *d*) Symmetrical (low viscosity) model data. For other symbols and information see the caption to figure 3.

The first series was designed to validate the code by direct comparison with experiment. The gas was assumed to be argon with a constant ratio of specific heats, $\gamma = \frac{5}{3}$. In order to make the comparison as accurate as possible, we used exactly the same input data (γ, ξ_i, θ) in each computation as had been used in the experiments, (table 3). We calculated (M_n, χ), and then compared the results with experiment (figures 3*a* and 3*b*) We also calculated (β_1, β_s) from the von Neumann theory and compared these results with experiment (figures 2*a* and 2*b*).

The second series was for $\langle \xi_i \rangle = 0.919$, or $\langle M_i \rangle = 1.035$, and there were four experimental points to compare with our calculations as shown in figures 4(*a*) and 4(*b*). The von Neumann theory of MR has no physically acceptable solutions for this series. The third series was for $\xi_i = 0.889737$, or $M_i = 1.0483$, for which we had one experimental point with $\theta = 10°$. For all three series i was a weak shock in the sense defined by both von Neumann and Henderson & Siegenthaler (tables 1 and 2).

Example of the field calculations corresponding to experiments with run numbers 85 and 81 are presented in figures 5 and 6, and in figure 7 we present our results for $\xi_i = 0.889737$ and $\theta = 10°$. The figure show the density contours for the entire flow

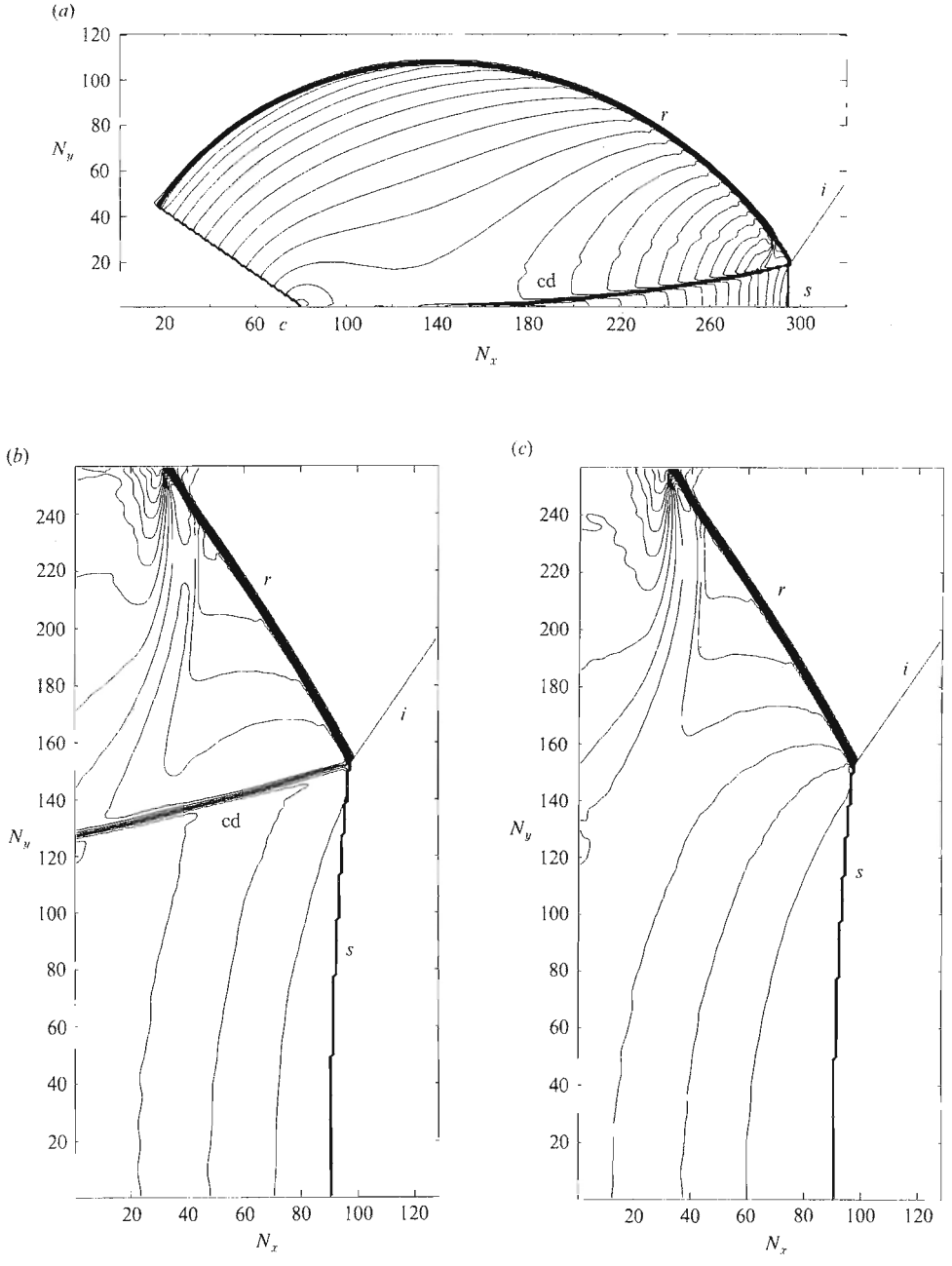

FIGURE 5(*a–c*). For caption see page 80.

field in each case, as well as enlargements of the density, pressure, and entropy contour plots in the interaction zones. The 'ripple' noticeable in most of the enlargements is due to a reflection condition we imposed at the top boundary, consequently, it is no more than an artefact of the calculations. It is not present for the timesteps in figures 5(*a*), 6(*a*), 7(*a*). Plots are also shown of the trajectory of the triple point. For each timestep, we plotted the location of the topmost point on the

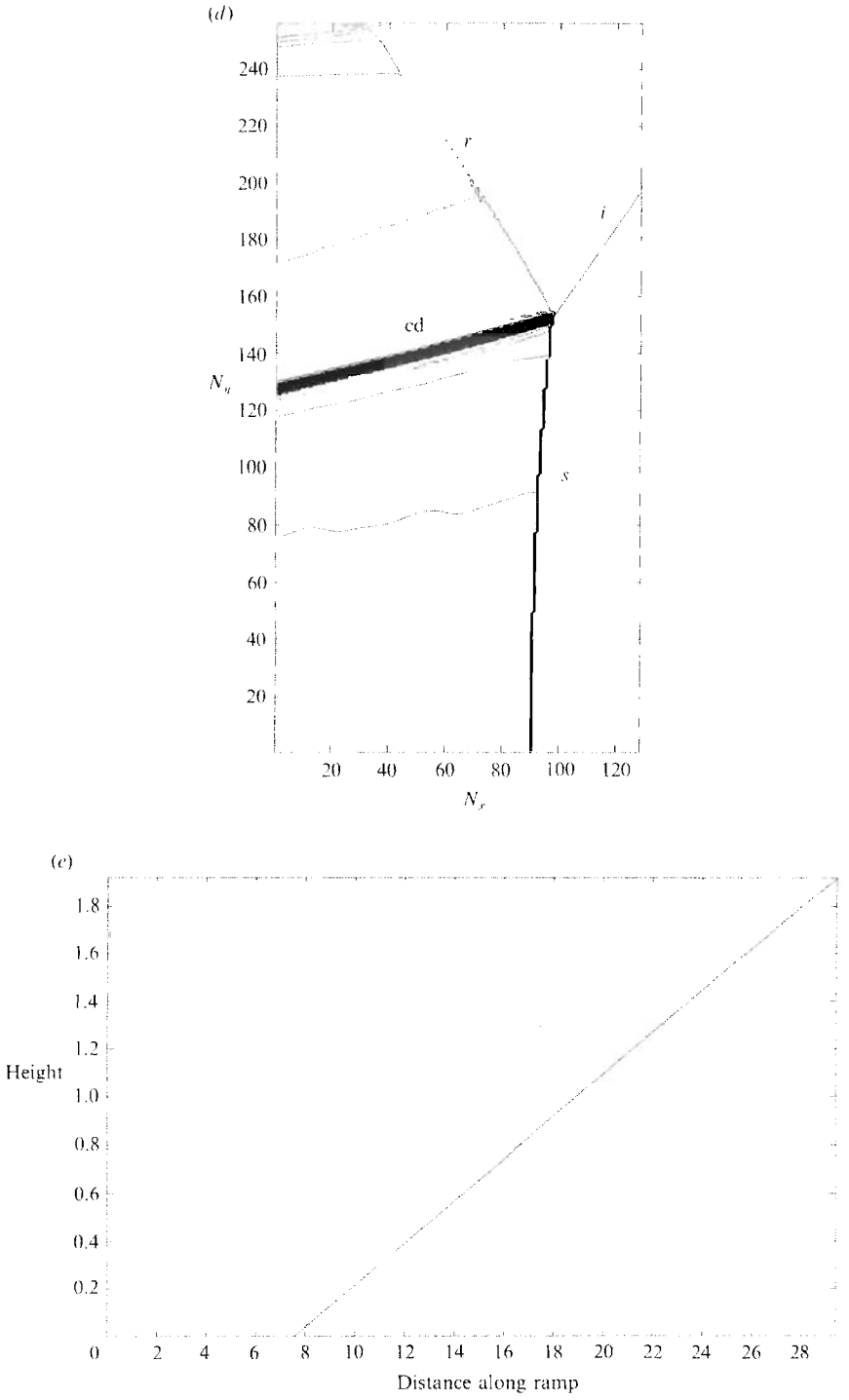

FIGURE 5. Finite difference calculations for the contours for the conditions of the weak Mach reflection with run number 85 in argon. $\gamma = \frac{5}{3}$, $\xi_i = 0.409$, $M_i = 1.47$, $\theta = 34.60°$. (*a*) Density contours for the entire field. (*b*) Enlargement of density contours in shock interaction region. (*c*) Enlargement of pressure contours. (*d*) Enlargement of entropy contours. (*e*) Trajectory of the triple point in the (x, y)-plane.

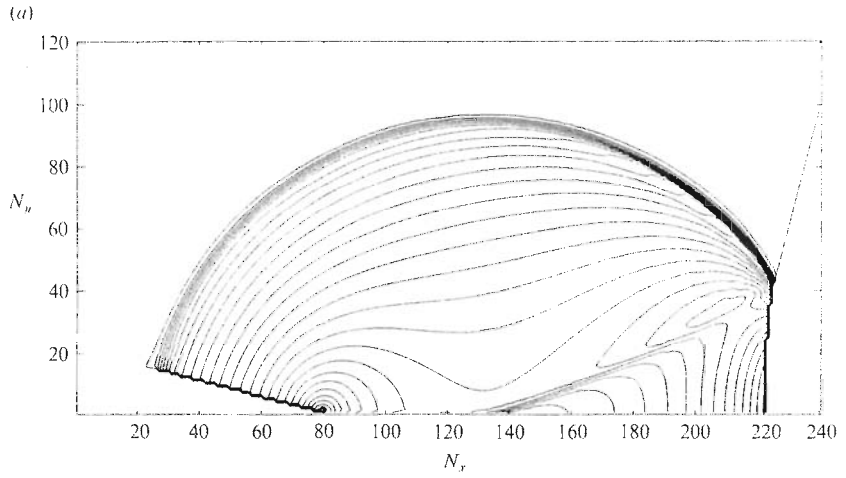

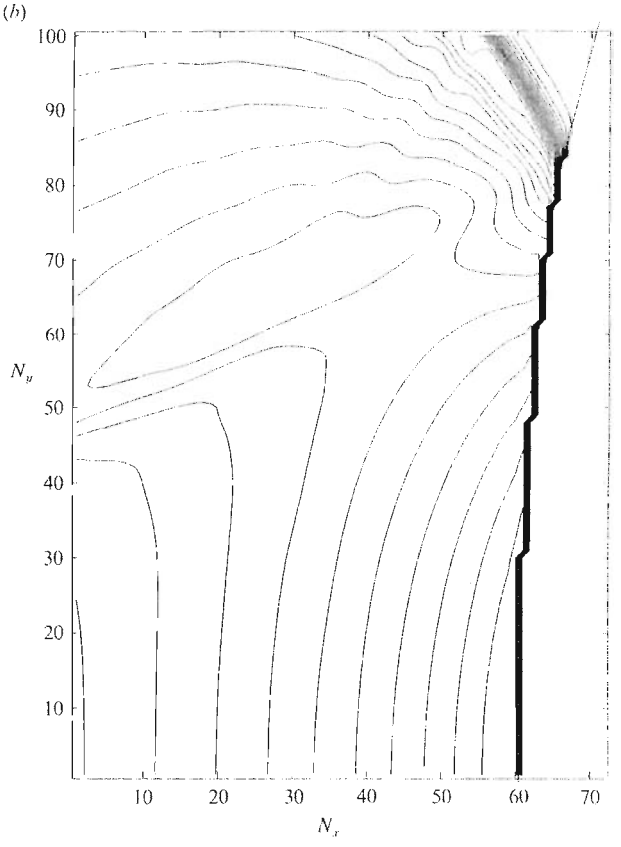

FIGURE 6(*a*, *b*). For caption see page 83.

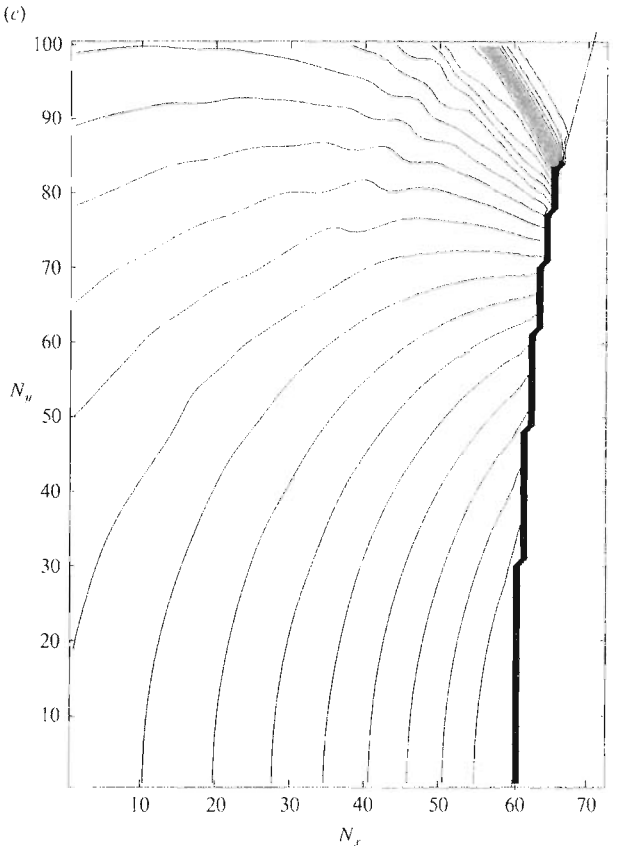

FIGURE 6(c). For caption see facing page.

tracked incident shock for which the post-shocked state differed from the state behind the incident shock. Also plotted as a solid line is a linear least-squares fit to the triple-point trajectory defined by these points.

The assessment of the numerical accuracy of the solutions obtained here is substantially simplified by the self-similarity of the problem. If the solution is self-similar, we expect that running the calculation for longer times should be the same as refining the grid. In fact, this is rigorously correct at the discrete level in the case of a uniform grid, in the sense that the solution depends on the spatial and temporal increments $\Delta x, \Delta y, \Delta t$ only in the ratios $\Delta x/\Delta t, \Delta y/\Delta t$. Our general approach has been to use the finest mesh that we could afford, and to monitor self-similarity by comparing the results at different times. The numerical triple-point trajectories are examples of such comparisons; our plots of the triple-point locations computed by the algorithm at every timestep is equivalent to producing the triple-point locations for a continuum of mesh spacings. The convergence of the discrete triple-point trajectories to a straight line indicates that our numerical calculations are converging to a self-similar solution to the equations. We have also performed other diagnostics, such as comparing contour plots of the solution at different times, and have seen similar convergence of the wave patterns.

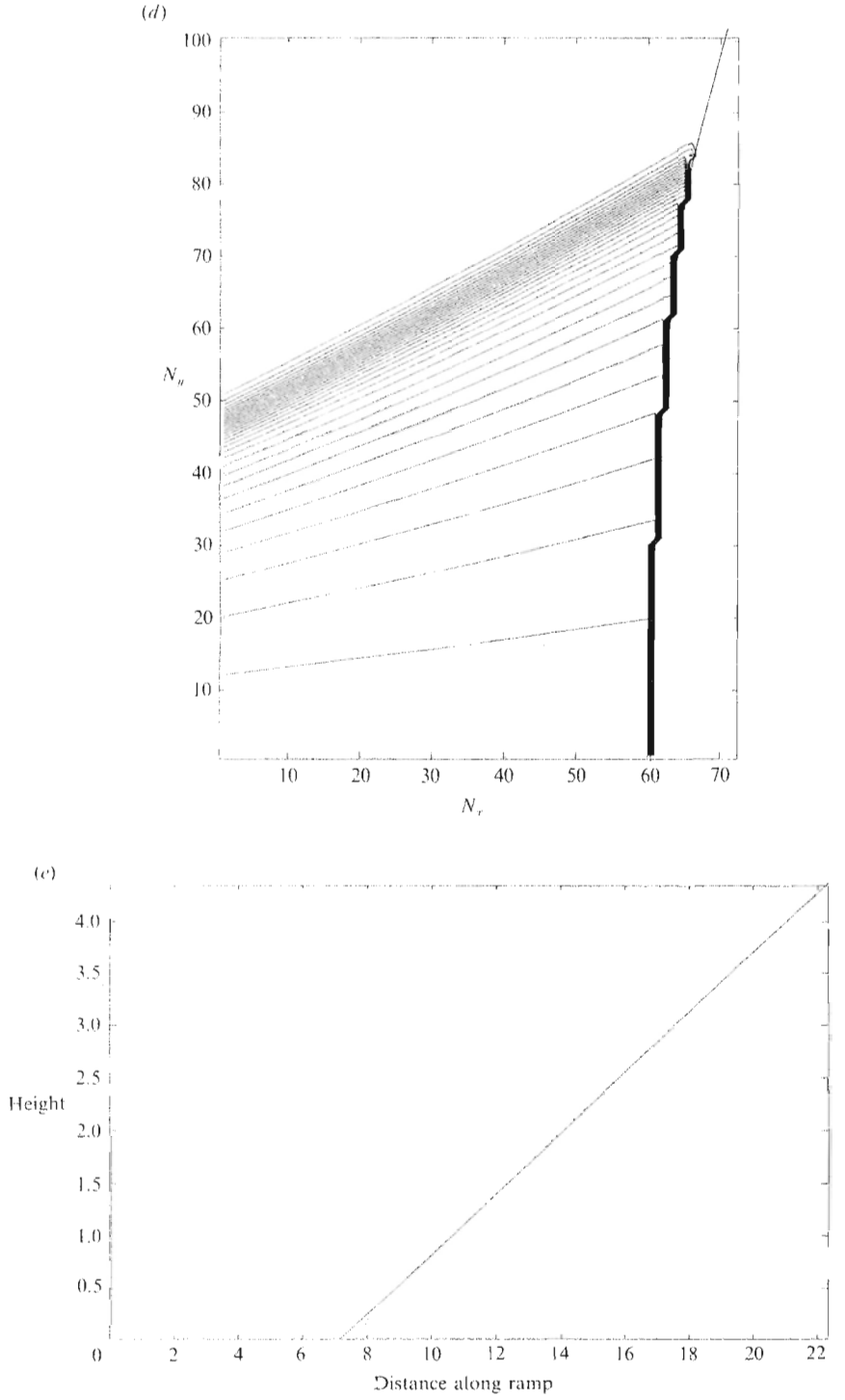

FIGURE 6. Finite difference calculations for the contours for the conditions of the von Neumann reflection with run number 81 in argon. $\gamma = \frac{5}{3}$. $\xi_i = 0.403$. $M_i = 1.48$. $\theta = 14.58°$. For these conditions the weak Mach reflection theory requires that $\beta_1 > \frac{1}{2}\pi$. For other information see the caption to figure 5.

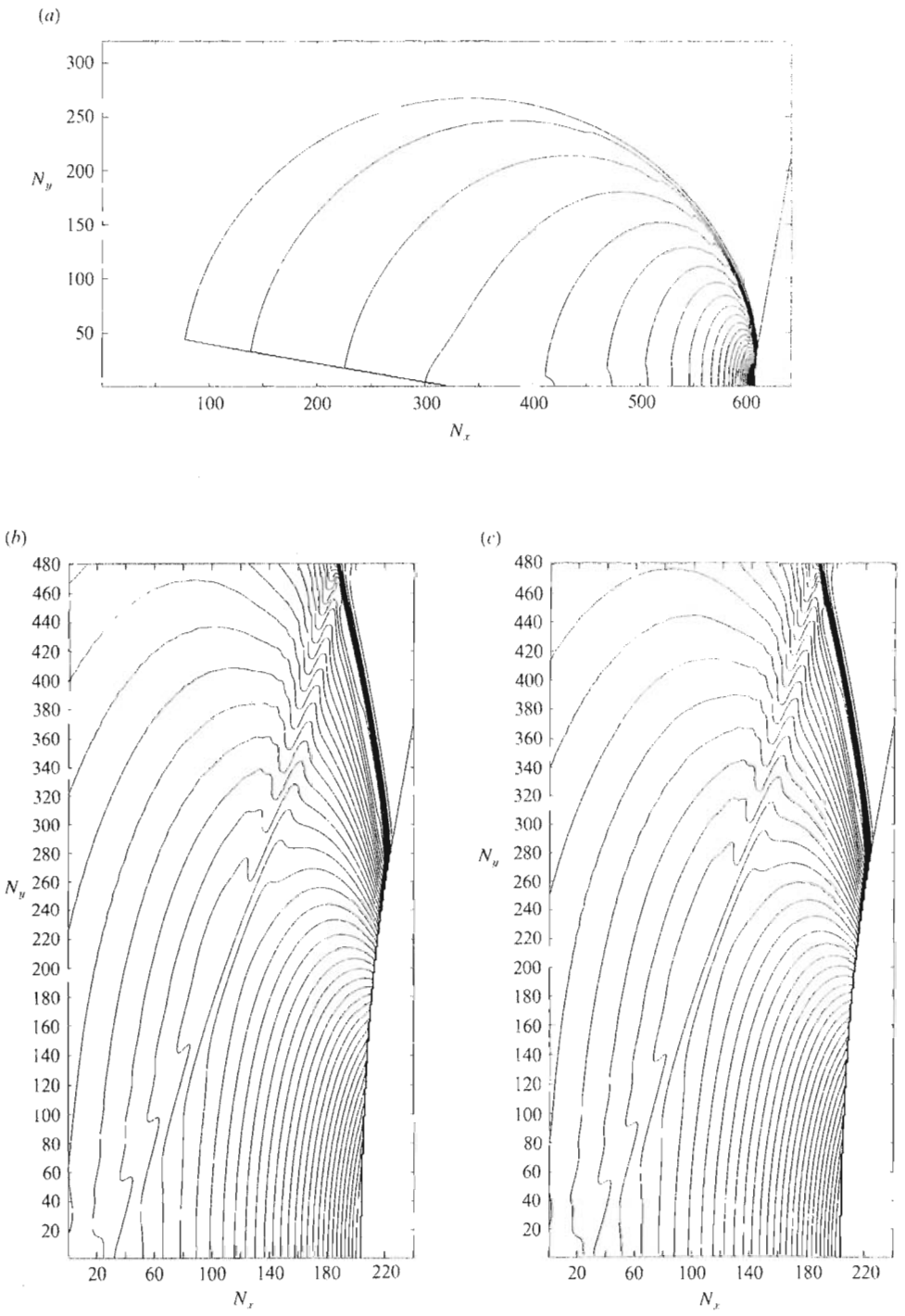

FIGURE 7(*a–c*). For caption see facing page.

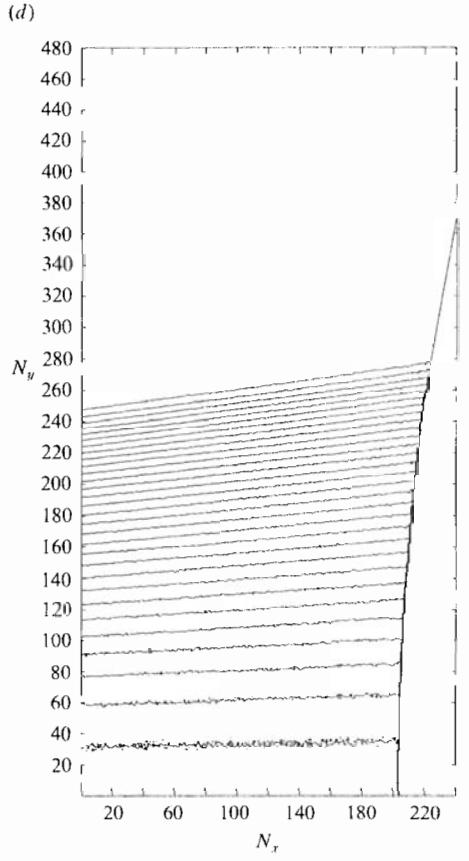

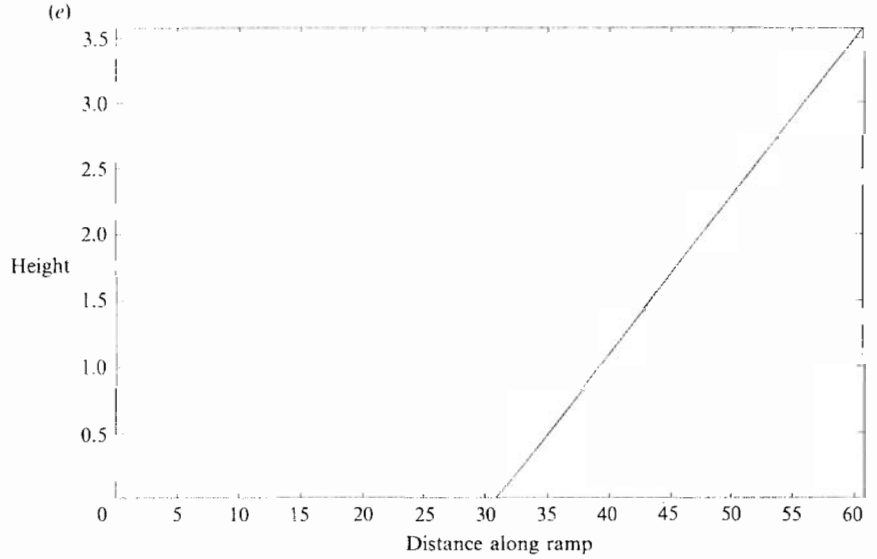

FIGURE 7. Finite difference calculations for the contours of a von Neumann reflection for which his theory has no acceptable Mach reflection solutions for argon. $\gamma = \frac{5}{3}$, $\xi_i = 0.889737$, $M_i = 1.0483$, $\theta = 10^c$. For other information see the caption to figure 5.

4. Discussion

4.1. *Comparison of the numerical results with experiment*

As already explained the most robust comparison was with the (M_n, χ) data (figures 3*a*, *b*, 4*a*, *b*). The agreement of the numerical data +, with the experimental data ⊙, is generally good for the $\langle M_i \rangle = 1.47$ results shown in figures 3(*a*) and 3(*b*). Indeed the agreement is within the limits of experimental error and computational uncertainty. However in spite of this, there is a small systematic discrepancy. The results shown in figures 4(*a*) and 4(*b*) are for much weaker incident shocks $\langle M_i \rangle = 1.035$ and here also the agreement is good. In this case the data is sparse and there is no sign of a systematic discrepancy.

We formed the hypothesis that the discrepancy evident in figures 3(*a*) and 3(*b*) was due to the viscosity of the argon, leading to shock–boundary-layer interactions. Another viscous effect was due to the (negative) displacement height of the boundary layer along the ramp. It was estimated to be only 0.02 mm at 5 cm downstream of the Mach shock, which made it immeasurably small. Our calculations, of course, were based on the assumption that the gas was inviscid. The flat plate forming the upstream part of the corner was 30 cm long and the Reynolds number there was about $Re \approx 4 \times 10^6$. A new series of models were designed to reduce the effects of viscosity, a typical one is illustrated in figure 1(*b*). While this design virtually eliminated shock–boundary-layer effects at the corner, there were still some residual sidewall boundary-layer effects. The same numerical data is compared with the experimental data from these symmetrical or 'low viscosity effects' models in figures 3(*c*, *d* and 4*c*, *d*). Generally, agreement is now excellent with no signs of any systematic discrepancy. Thus when precautions are taken to minimize the effects of viscosity, the numerical results agree with experiment. We conclude that these results validate the code.

4.2. *Comparison of the von Neumann theory of MR with experiment*

The von Neumann theory has physically acceptable solutions of MR for the $\langle M_i \rangle = 1.47$ series, but not for the weaker series $\langle M_i \rangle = 1.035$. It is impossible to calculate (M_n, χ) from this theory, so it is necessary instead to calculate the wave angles (β_1, β_s) to compare with experiment. The data for the concave corner models are presented in figures 2(*a*) and 2(*b*). Although the theory approaches agreement with experiment near transition to RR, $\theta \to \theta^*$, there is an increasingly large discrepancy in the other direction as θ becomes smaller. For the experimental data it will be noticed that the reflected wave angle β_1 is always such that $\beta_1 \leqslant \frac{1}{2}\pi$; therefore *by experiment* the reflected wave r is never inclined forward of the triple point; it must always be either a backward facing shock $\beta_1 < \frac{1}{2}\pi$, or, at most, a normal shock, $\beta_1 = \frac{1}{2}\pi$.

The same comparisons are made with the symmetrical model data in figures 2(*c*) and 2(*d*). For $\beta_1 < \frac{1}{2}\pi$ it will be noticed that the discrepancies are reduced by about half compared with the concave corner data (figures 2*a* and 2*b*). This demonstrates the sensitivity of the angle data to viscous effects and indeed to small variations in the system parameters. Apart from this observation, the conclusions are the same as before. These considerations suggested the following hypotheses to us.

(*a*) When $\beta_1 < \frac{1}{2}\pi$, for the von Neumann theory, then it will agree with experiment, provided that the effects of viscosity can be sufficiently reduced in the experiments.

(*b*) When $\beta_1 > \frac{1}{2}\pi$, for the theory, that is when the reflected wave is required to be inclined forward of the triple point, then the theory will *not* agree with experiment.

(*c*) When the theory has no physically acceptable solutions, for example the solutions may be unreal, or may require the reflected wave to be an expansion shock, then here also it will *not* agree with experiment.

If the hypotheses are true then there must be at least two irregular reflections. These are a classical Mach reflection as described by the von Neumann theory but restricted to $\beta_1 \leqslant \frac{1}{2}\pi$, and to solutions that are otherwise physically realistic, and another system which we will name a 'von Neumann reflection' (NR), which exists when the theory fails. Clearly the transition condition for MR → NR, is

$$\beta_1 = \tfrac{1}{2}\pi. \tag{3}$$

According to the hypotheses the experiments listed in table 3 for the $\langle M_i \rangle = 1.47$ series, and with run numbers 81–84 are von Neumann reflections while 85–100 are weak Mach reflections. This may be verified by inspection of figure 2 using table 3 and equation (3). All of the experiments in the $\langle M_i \rangle = 1.035$ series are von Neumann reflections. A schlieren photograph of a weak MR from run number 85 is presented in figure 8. A similar photograph of an NR for which the theory requires $\beta_1 > \frac{1}{2}\pi$ is presented in figure 9 (run number 81). Finally a photograph of an NR for which the theory has no real solutions is presented in figure 10.

4.3. *Comparison of the von Neumann theory of MR with the numerical data*

We shall now test hypothesis (*a*) of the previous section. We shall make an indirect comparison with experiment. Since we have already validated the code by showing that the numerical data from it are in good agreement with experiment (figures 3 and 4), then by comparing the von Neumann theory with the code data it may be determined indirectly if the theory agrees with experiment. For example the pressure ratio P_2/P_0 across the incident and reflected shocks can be calculated for the values of (γ, ξ_i, θ) corresponding to experiments 85–100 using both the code and the von Neumann theory. The results are shown in table 4 and they agree within 1 %. We find that this comparison is robust (not sensitive to small variations in the system parameters or to viscosity). The streamline direction angle δ_2 of the flow downstream of the reflected shock can be found in the same way (table 4). In this case the code displays more sensitivity which causes some uncertainty in δ_2. Nevertheless the results do bracket the von Neumann data. Therefore the data shown in table 4 supports hypothesis (*a*).

4.4. *The structure of the von Neumann reflection NR*

Hypotheses (*b*) and (*c*) will be considered here together. An MR will be replaced by an NR whenever the von Neumann theory either requires that $\beta_1 > \frac{1}{2}\pi$ or when it has no physically acceptable solutions. At first glance the photographs of an NR (figures 9 and 10) appear to be those of a typical MR. However careful examination reveals some important differences. Thus the incident and Mach shocks appear to be a single wave with a smoothly turning tangent near the triple point, whereas an MR (figure 8) has a slope discontinuity between those two shocks at the triple point. Furthermore the contact discontinuity has a quite sharp appearance in the MR, but a fuzzy appearance in NR as though it was a distributed shear layer rather than a shear discontinuity. The contours plotted from the code calculations show a similar behaviour. For example the detailed entropy contours for the MR of experiment 85 (figure 5*d*) display a concentrated band of entropy emanting from the triple point, and a clearly defined entropy jump across the reflected shock. The curvature of the Mach shock near the triple point is also noticeably large. On the other hand, the

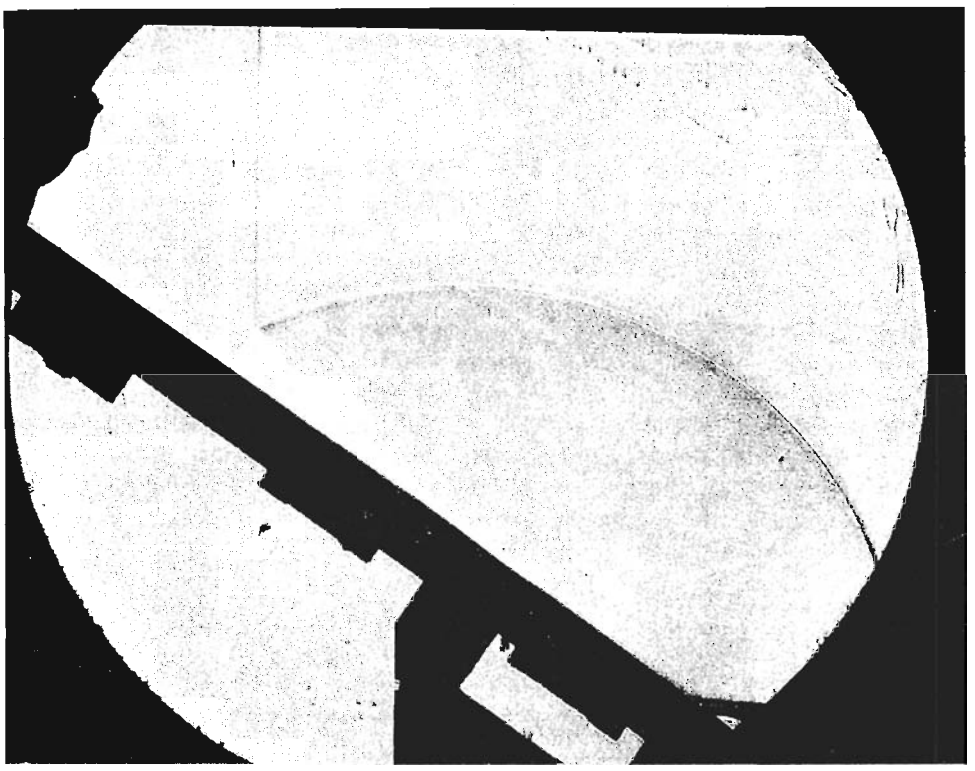

FIGURE 8. Schlieren photograph of a weak Mach reflection over a concave corner model in argon for run number 85. $\gamma = \frac{5}{3}$, $\xi_i = 0.409$, $M_i = 1.47$, $\theta = 34.60$.

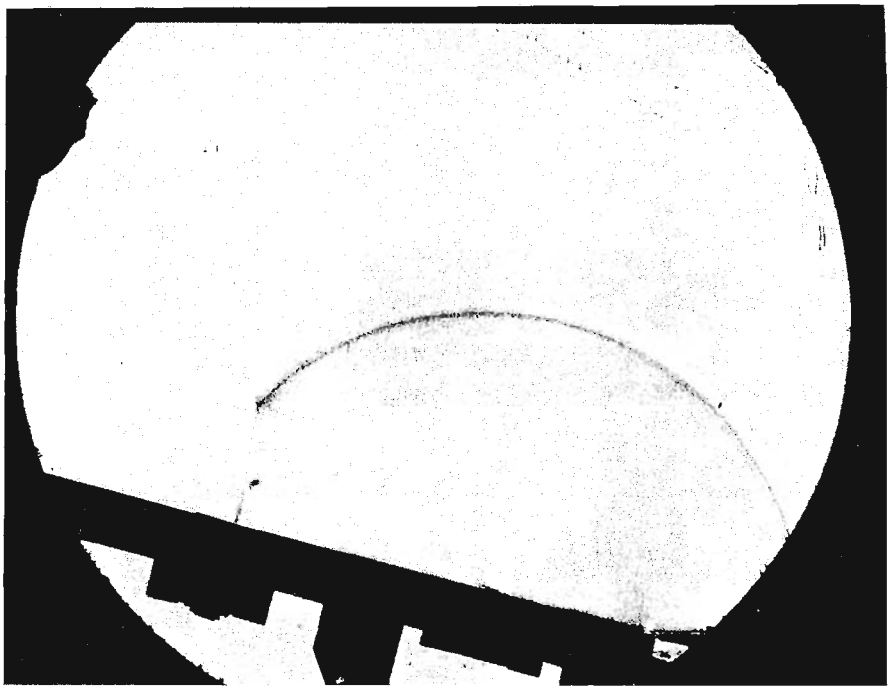

FIGURE 9. Schlieren photograph of a von Neumann reflection over a concave corner model in argon for run number 81. In this case the theory of weak MR requires that $\beta_1 > \frac{1}{2}\pi$. $\gamma = \frac{5}{3}$. $\xi_i = 0.403$. $M_i = 1.48$. $\theta = 14.58°$.

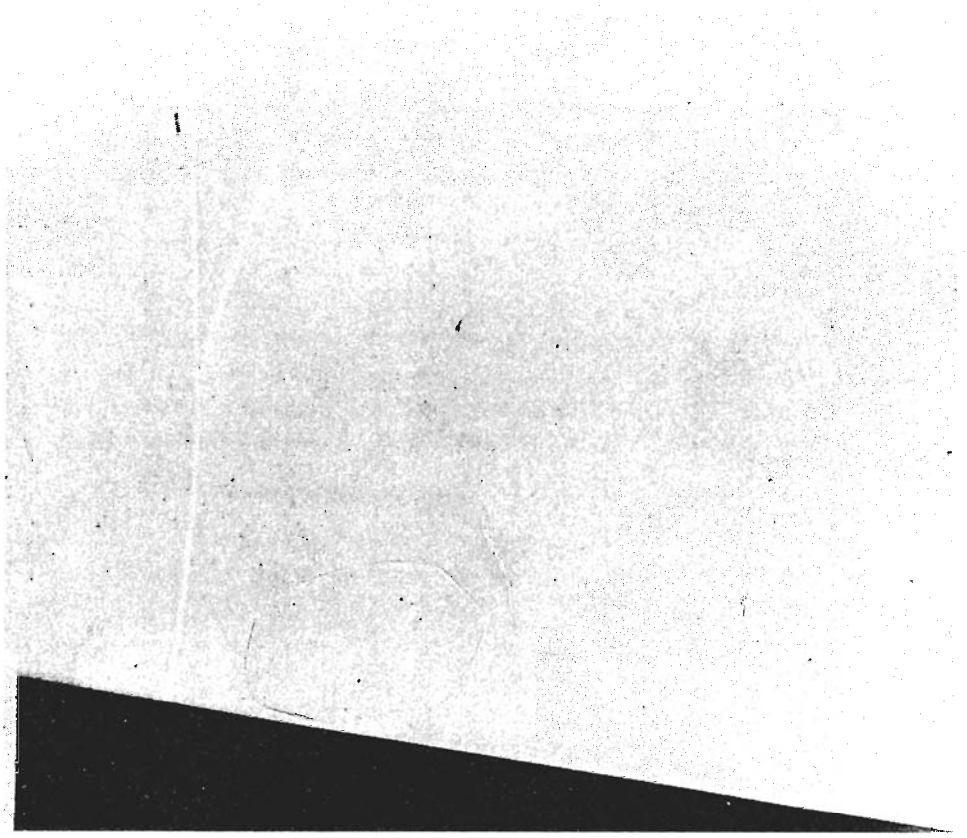

FIGURE 10. Schlieren photograph of a von Neumann reflection over a concave model in argon for which Mach reflection has no physically acceptable solutions. $\gamma = \frac{5}{3}$, $\xi_i = 0.889$, $M_i = 1.05$, $\theta = 10°$.

Run no.	85	86	87	100
$\theta°$	34.60	38.68	44.48	47.55
ξ_i	0.409	0.405	0.400	0.400
M_i	1.47	1.47	1.48	1.48
P_2/P_0 data from computer code	4.0984	4.6397	5.4612	5.888
P_2/P_0 data from von Neumann theory	4.1191	4.6167	5.4347	5.9315
$\delta_2°$ data from computer code	17.03–19.01	12.93–14.71	6.62–8.25	3.19–4.78
$\delta_2°$ data from von Neumann theory	17.90	13.61	7.12	3.58

TABLE 4. Comparison of the von Neumann theory with the computer code

contours corresponding to the NR of experiment 81 (figure 6*d*) display a smoothly distributed band of entropy with no sign of an entropy jump across the reflection even though it obeys the RH conditions. We presume that the jump is too small to be resolved by the calculations. The curvature of the Mach shock is now much smaller than that shown in figure 5(*d*), and the triple point has now become somewhat indefinite.† We infer that the reflection is not a shock but a smoothly

† In that event, we calculated χ at the point where the leading edge of the reflection first encountered *i*.

distributed self-similar compression in the region where it interacts with the incident/Mach shocks. Evidence of the self-similarity in the region is found in the linear character of the triple point trajectory except for the immediate vicinity of the corner (figure 6*e*).

The conclusions remain the same when the incident shock is so weak that there are no real solutions to the von Neumann theory (hypothesis (*c*)). In the example shown in figure 7(*d*) the smoothness of the field is evident and so also is the finite curvature of the Mach shock. It is also evident in figure 7(*c*) for the pressure contours how the reflection steepens into a shock as it retreats from the incident/Mach shock interaction zone.

4.5. *Behaviour of the irregular reflections near their transition* $\beta_1 = \frac{1}{2}\pi$

Suppose that initially we have a weak MR, then it follows by hypothesis (*a*) that $\beta_1 \leqslant \frac{1}{2}\pi$, the reflected wave is a shock and there is a well-defined triple point. The streamline deflection angle δ_2 across the reflected shock can be calculated from (Ames 1953).

$$\delta_2(P_2) = \delta_1 + \tan^{-1}\left\{\frac{P_2/P_1 - 1}{\gamma M_1^2 - P_2/P_1 - 1}\left[\frac{(1+\mu^2)(M^2-1)-(P_2/P_1-1)}{P_2/P_1+\mu^2}\right]^{\frac{1}{2}}\right\}. \tag{4}$$

where $\mu^2 \equiv (\gamma-1)/(\gamma+1)$, and M_1 is the free-stream Mach number between the incident and reflected shocks. Now the reflected wave becomes a normal shock as the system approaches the transition $\beta_1 \to \frac{1}{2}\pi$, and at this condition $P_2 = P_n$, say. Then with (γ, M_1, δ_1) held constant we may obtain from (4) without difficulty,

$$\frac{\partial \delta_2}{\partial P_2} \sim (P_2 - P_n)^{-\frac{1}{2}}. \tag{5}$$

So the streamline direction changes rapidly with pressure as transition is approached, MR → NR. This partly explains why the pressure data is so robust while the streamline deflection data is so sensitive (table 4). These quantities are of course ultimately functions of the system parameters (γ, ξ_i, θ). The wave angles (β_1, β_s) also show marked sensitivity as MR → NR. (figure 2) which is evidently, at least in part, another manifestation of the singularity (5) since they are also functions of the same parameters. However, the experimental data for (β_1, β_s) shown in figure 2 also show marked sensitivity to the effects of viscosity whereas the (M_n, χ) data do not (figure 3). Indeed the experiments indicate that sensitivity to viscosity is the dominant effect for most of the range of $\beta_1 < \frac{1}{2}\pi$ data in figure 2, the sensitivity due to the singularity is presumably mostly confined to the vicinity of the transition point $\beta_1 = \frac{1}{2}\pi$.

A dynamical mechanism for the formation of the distributed reflected compression in NR is suggested by the way in which the three-shock theory fails. Given the triple-point trajectory path in MR one can use the theory to calculate the entire family of reflected shocks that satisfy $P_2 \leqslant P_n$, and assuming that MR solutions exist in the NR parameter space then these shocks must be forward facing, $\beta_1 > \frac{1}{2}\pi$. If we now override this condition and impose the requirement that the reflected shocks must be backward facing in order to conform with experiment (figure 2), then we find that the flow direction δ_s, downstream of the Mach shock diverges from that δ_2 downstream of the reflected shock (figure 11). This suggests that in NR the flow behind the Mach shock acts like a distributed sink of fluid which weakens the reflection and turns its direction of propagation. The result is that it becomes a distributed compression where it is near the incident/Mach shocks (compare figures 5 and 7). The self-similar

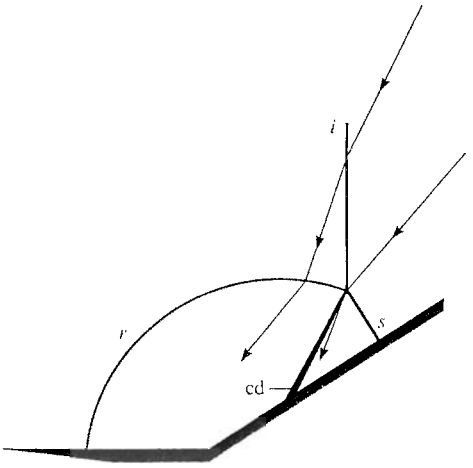

FIGURE 11. The streamline divergence near the shock triple point.

velocity vector normal to the leading edge of the reflection is either sonic or subsonic; we do not have enough evidence to make a definite determination. But as already noted the compression does steepen into a shock as it retreats from the incident/Mach shocks. The distance over which this happens is typically quite small and is only just detectable in the results shown in figure 7(*c*), which is one of our most finely resolved numerical studies of a very weak NR system. We expected the distance to scale with the divergence of the streamline angles near the interaction region, which is itself typically quite small. It will be noted that there are large curvatures of the reflection in this region, just as there is in MR near the transition MR → NR. This is most evident in the pressure contours (figure 7*c*) where the direction of the reflection turns sharply in the vertical direction as it approaches the incident/Mach shocks. Finally we remark that the mechanism is both inviscid, and compatible with self-similarity.

4.6. *Conditions at transition*

4.6.1. *MR⇌NR*

This transition has already been discussed and its criterion which is given by equation (3). $\beta_1 = \frac{1}{2}\pi$ has been noted. When it may be assumed that the reflection system is propagating in a perfect gas then (3) can be more conveniently expressed in terms of the system parameters (γ, ξ_i, θ) as follows (Henderson 1987), if $x \equiv \sin^2 \omega_a$, where ω_a is the angle of incidence of the incident shock to the surface when the reflected wave is a normal shock and θ at this point is $\theta_a = \frac{1}{2}\pi - \omega_a$, then

$$C_2 x^2 + C_1 x + C_0 = 0, \tag{6}$$

where

$$C_2 \equiv 2\gamma[(\gamma+1)+(\gamma-1)\,\xi_i]\,(1-\xi_i)\,[(\gamma+1)+(\gamma+3)\,\xi_i], \tag{7a}$$

$$C_1 \equiv -\{(\gamma+1)^2(3\gamma+1)+(\gamma+1)(\gamma^3+3\gamma^2+3\gamma-3)\,\xi_i + (2\gamma^4+3\gamma^3-9\gamma^2-15\gamma+3)\,\xi_i^2+(\gamma^4+2\gamma^3-4\gamma^2+10\gamma-1)\,\xi_i^4\}, \tag{7b}$$

$$C_0 \equiv [(\gamma+1)+(\gamma-1)\,\xi_i]^3, \tag{7c}$$

and where the negative branch of (6) provides the root of physical significance.

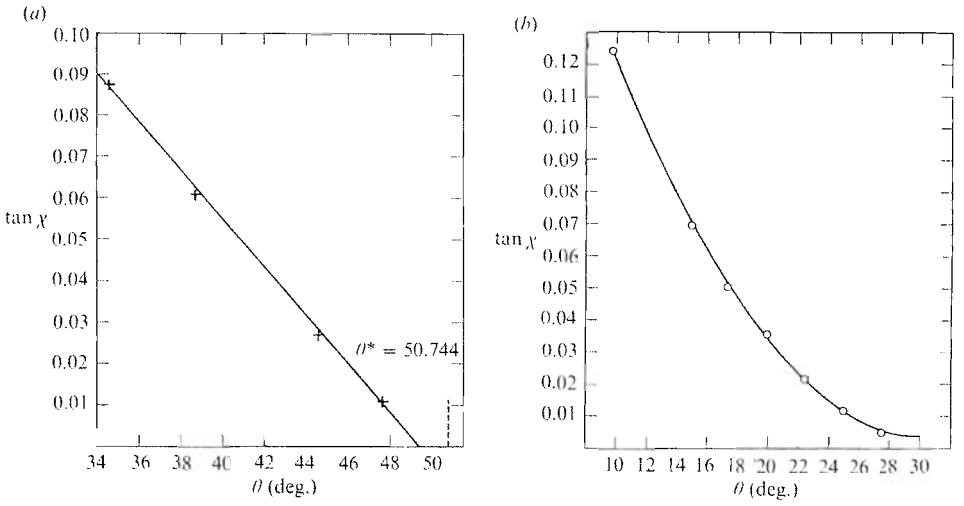

FIGURE 12. Computation of the regular–irregular transition point for weak shock waves. (*a*) Data selected from either figures 3(*b*) or 3(*d*) for MR → RR, with a linear curve of best fit. (*b*) Computational data for NR → RR, for $\gamma = \frac{5}{3}$, $\xi_i = 0.889737$, $M_i = 1.0483$, $\theta = 10°$ with a quadratic correlation curve. The curve is terminated at the point where $\tan\chi$ is a minimum, i.e. $\theta \approx 30.2°$.

4.6.2. *MR → RR*

In this case the results from the code and the experiments show that the non-dimensional height $\tan\chi$ of the Mach shock approaches zero (its transition point) linearly as θ increases. This is demonstrated in figure 12(*a*), which is a replot of the MT data from figure 3(*d*). After extrapolating to the value of θ for which $\tan\chi = 0$ we get $\theta \approx 49\frac{1}{4}$ which is approximately equal to $\theta = 50.744°$, obtained for the sonic/detachment point calculated from the von Neumann theory.

4.6.3. *NR → RR*

The data for NR is replotted from figure 4(*d*) in figure 12(*b*). We obtained a least-squares quadratic fit to the data, which means, of course, that $\tan\chi$ approaches zero quadratically with increasing θ in the case of NR. The fit to the data was cut off at the minimum computed value of $\tan\chi$, this was at $\theta \approx 30.2°$ compared to the sonic/detachment value of $\theta = 30.4173°$.

We see that for the inverse transition RR → NR, there is initially a very slow growth in the height of the Mach shock ($\tan\chi$) with decreasing θ. This may help to account for the apparent persistence of RR into the NR parameter space. In other words, the height of the Mach shock may be too small for it to be optically resolvable until θ has become a few degrees smaller than the sonic/detachment transition angle θ^*. Certainly there is no sign of the persistence in figure 12(*b*) where the fit terminates almost exactly at θ^*.

5. Conclusions

(1) Our code calculations of the flows in weak, irregular, reflections were based on the continuity, and Euler equations for the unsteady, two-dimensional, compressible, inviscid, flow of a perfect gas, where all the waves were required to satisfy the

Rankine–Hugoniot jump conditions. The comparison between the numerical and the experimental data for the ramp shock Mach number M_n, and the triple-point trajectory path angle χ, gave excellent agreement especially when precautions were taken to reduce the effects of viscosity on the experimental data (figures 3 and 4). It was concluded that the comparison validated the code.

(2) It is impossible to calculate (M_n, χ) from the inviscid von Neumann theory of weak MR in order to compare with experiment. So we calculated the wave angles (β_1, β_s) to make the comparison and it revealed large discrepancies (figure 2). The experiments showed firstly that the reflected wave was never inclined forward of the triple point, $\beta_1 \leqslant \frac{1}{2}\pi$, and secondly that the data was sensitive to viscous effects. We concluded that the von Neumann theory would agree with experiment (or very nearly so) if the following conditions were met,

(*a*) The theory satisfied, $\beta_1 \leqslant \frac{1}{2}\pi$.

(*b*) The theory provided real solutions, and did not require there to be any expansion shocks in the wave system.

(*c*) Precautions were taken to minimize the effects of viscosity on the experimental data.

Further evidence to support the validity of the von Neumann theory under these conditions was provided by comparing it with the numerical results. In particular we found that the theory agreed within 1% with the code for the pressure P_2 downstream of the reflected shock. It also agreed with the streamline direction data δ_2 (table 4), although these data showed sensitivity to variations in the parameters (γ, ξ_i, θ) especially when $\beta_1 \to \frac{1}{2}\pi$. This was traced to a singularity at this condition of the form,

$$\frac{\partial \delta_2}{\partial P_2} \sim (P_2 - P_n)^{\frac{1}{2}},$$

which explained why the pressure data was robust while the angle data was sensitive. On the other hand, the experimental data showed that the angle data (β_1, β_s) was sensitive to the effects of viscosity, while the (M_n, χ) were insensitive (robust).

(3) When the von Neumann theory failed, it was concluded that the weak Mach reflection was transformed into a new type of irregular reflection which we called a von Neumann reflection (NR). In this system the incident and Mach shocks appear to form a single wave with a continuously turning tangent. The reflection is a smoothly distributed and apparently self-similar pressure disturbance near its interaction region with the incident/Mach shocks, but it steepens into a shock as it retreats from them.

This work was performed under the auspices of the US Department of Energy at the Lawrence Livermore National Laboratory under contract W-7405-Eng-48. Partial support under contract W-7405-Eng-48 was provided by the Applied Mathematical Sciences Program of the Office of Energy Research.

REFERENCES

Ames Research Staff 1953 Equations, tables and charts for compressible flow. *NACA Ref.* 1135.

Berger, M. & Colella, P. 1987 Adaptive mesh refinement for shock hydrodynamics. Lawrence Livermore National Laboratory. Preprint UCRL 97196, to appear in *J. Comp. Phys.*

Birkhoff, G. 1950 *Hydrodynamics, A Study in Logic, Fact and Similitude.* Princeton University Press.

Bleakney, W. & Taub, A. H. 1949 *Rev. Mod. Phys.* **21**, 584–605.

CHERN, I. L. & COLELLA, P. 1987 A conservative front tracking method for hyperbolic conservation laws. Lawrence Livermore National Laboratory, Preprint UCRL-97200.

COLELLA, P. 1984 Multidimensional upwind methods for hyperbolic conservation laws. Lawrence Berkeley Lab. Rep. LBL-17023, to appear in *J. Comp. Phys.*

COLELLA, P. & WOODWARD, P. R. 1984 *J. Comp. Phys.* **54**, P175–201.

GLAZ, H. M., COLELLA, P., GLASS, I. & DESCHAMBAULT, R. 1985 *Proc. Roy. Soc. Lond.* A **398**, P117–140.

HENDERSON, L. F. 1987 *Z. angew. Math. Mech.* **67**, 73–86.

HENDERSON, L. F. & GRAY, P. M. 1981 *Proc. Roy. Soc. Lond.* A **377**, 363–378.

HENDERSON, L. F. & LOZZI, A. 1975 *J. Fluid Mech.* **68**, 139–155.

HENDERSON, L. F. & LOZZI, A. 1979 *J. Fluid Mech.* **94**, 541–560.

HENDERSON, L. F. & SIEGENTHALER, A. 1980 *Proc. Roy. Soc. Lond.* A **369**, 537–555.

HORNUNG, H. G. & KYCHAKOFF, G. 1977 *Proc. 11th Intl Symp. Shock Tubes & Waves, Seattle*, pp. 296–302.

HORNUNG, H. G., OERTEL, H. & SANDEMAN, R. J. 1979 *J. Fluid Mech.* **90**, 541–560.

HORNUNG, H. G. & ROBINSON, M. H. 1982 *J. Fluid Mech.* **123**, 155–164.

HORNUNG, H. G. & TAYLOR, J. R. 1982 *J. Fluid Mech.* **123**, 143–153.

JOHANNESEN, N. H. & HODGSON, J. P. 1979 *Rept. Prog. Phys.* **42**, 629–676.

KAWAMURA, R. & SAITO, H. 1956 *J. Phys. Soc. Japan* **11**, 584–542.

LEER, B. VAN 1979 *J. Comp. Phys.* **32**, 276–303.

MÖLDER, S. 1971 *CASI Trans.* **4**, 73–80.

NEUMANN, J. VON 1943 See *Collected Works*, vol. 6, 1963. Pergamon.

PANTAZAPOL, D., BELLETT, J. C. & SOUSTRE, J. 1972 *C.R. Acad. Sci. Paris*, A **255**, 275g.

WOODWARD, R. R. & COLELLA, P. 1984 *J. Comp. Phys.* **54**, 115–174.